Signal Processing 32 (1993) 343-355
Elsevier

A multiresolution nonrectangular wavelet representation for two-dimensional signals*

A. Enis Çetin (member EURASIP)
Department of Electrical and Electronics Engineering, Bilkent University, Bilkent 06533, Ankara, Turkey

Received 9 July 1991
Revised 24 February 1992, 5 June 1992 and 16 October 1992

Abstract. In this paper, a new multiresolution wavelet representation for two-dimensional signals is described. This wavelet representation is based on a nonrectangular decomposition of the frequency domain. The decomposition can be implemented by a digital filter bank. The application of the new representation to the coding of quincunx and rectangularly sampled images is considered and simulation examples are presented.

Zusammenfassung. In dieser Arbeit wird eine neuartige Mehrfachauflösungs-Waveletdarstellung für zweidimensionale Signale beschrieben. Diese Wavelet-Darstellung beruht auf einer nicht-rechteckigen Zerlegung des Frequenzbereichs. Die Zerlegung kann mittels einer digitalen Filterbank implementiert werden. Wir diskutieren die Anwendung der neuen Darstellung auf die Codierung von quincunx- und rechteckig abgetasteten Bildern und beschreiben Simulationsbeispiele.

Résumé. Une représentation multi-résolution par ondelettes originale est décrite dans cet article. Cette représentation par ondelettes est basée sur une décomposition non rectangulaire du domaine fréquentiel. La décomposition peut être implantée par un banc de filtres digitaux. Cette représentation est appliquée au codage d'images échantillonnées rectangulairement et en quinconce et des exemples de simulation sont présentés.

Keywords. Wavelets; subband decomposition; image coding.

1. Introduction

Multiresolution representation of signals is used in many interesting fields including image analysis, video and image coding, and geophysics. In image coding [16], the original image is decomposed into several subimages at low resolutions and coding algorithms are applied to these low resolution images. In image analysis, many methods have been developed to process an image at different resolution levels [5, 12, 16].

Recently, Mallat [12, 13] developed a framework which unified the wavelet theory [14] and subband decomposition based multiresolution signal representation methods. Wavelets which are obtained from a single function by dilations and translations constitute an orthonormal basis of $L^2(\mathbb{R})$, and provide a representation of any function in $L^2(\mathbb{R})$. Mallat also introduced a two-dimensional (2-D) wavelet representation and 2-D discrete wavelet transform in order to deal with 2-D discrete-time signals which are sampled on a rectangular grid. This wavelet representation has a resolution factor of 2.

Correspondence to: Professor A. Enis Çetin, Department of Electrical and Electronics Engineering, Bilkent University, Bilkent 06533, Ankara, Turkey. Tel.: (90) 4 266 4307; Fax: (90) 4 266 4127; E-mail: cetin@trbilun.bitnet

* This work is presented in part in the Bilkent International Conference on New Trends in Communication, Control, and Signal Processing, 2–5 July 1990, Ankara, Turkey. Proceedings of this conference are published as Communication, Control, and Signal Processing, E. Arikan, Editor, Elsevier Science Publishers, The Netherlands, 1990. This work is supported by TÜBITAK, Turkey.

In many image transmission systems 2-D signals are sampled on nonrectangular sampling grids such as the line quincunx grid and hexagonal grids [1, 2, 8, 11, 15]. This paper extends the wavelet represention to the case of quincunx sampled 2-D signals. The implementation of this representation can be carried out in discrete-space domain by the nonrectangular subband decomposition filter bank developed by Ansari et al. [2]. This filter bank consists of a 2-D IIR highpass filter and a lowpass filter which have diamond shaped passband and stopband, respectively. In this paper, the application of the new wavelet representation to the coding of quincunx and rectangularly sampled images is considered and simulation examples are presented.

Recently, a similar class of wavelet representation with a resolution factor of $\sqrt{2}$ was independently introduced in [10, 9]. In [9] the focus was on some computer vision and image analysis problem. In both [10] and [9] FIR filters were used to construct a nonrectangular wavelet representation.

2. A multiresolution approximation of $L^2(\mathbb{R}^2)$

We say that the sequence of closed subspaced $\{U_l,\ l\in\mathbb{Z}\}$ is a nonrectangular multiresolution approximation of $L^2(\mathbb{R})$, if the following conditions hold:

1. $U_l\subset U_{l+1}$ for all $l\in\mathbb{Z}$.
2. $\lim_{l\to\infty} U_l$ is dense in $L^2(\mathbb{R}^2)$ and $\lim_{l\to-\infty} U_l=\{0\}$.
3. If $f(\boldsymbol{X})\in U_l$ then $f(\Lambda\boldsymbol{x})\in U_{l+1}$, for all $l\in\mathbb{Z}$, where

$$\Lambda=\begin{bmatrix}1 & 1\\ 1 & -1\end{bmatrix}, \tag{1}$$

   $\boldsymbol{x}=(x_1, x_2)$ and $f(\Lambda\boldsymbol{x})=f(x_1+x_2, x_1-x_2)$ (with somewhat abuse of notation).
4. $f(\boldsymbol{x})\in U_l$ implies that $f(\boldsymbol{x}-\Lambda^{-l}\boldsymbol{k})\in U_l$, for all $\boldsymbol{k}\in\mathbb{Z}^2$.
5. There exists an isomorphism I from U_0 onto $\ell^2(\mathbb{Z}^2)$. This isomorphism is defined as in [13].

The following result shows that one can construct an orthonormal basis of the subspace U_l by properly translating and scaling a function, $\varphi(\boldsymbol{x})$.

RESULT 1. Let $\{U_l\}$ be a nonrectangular multiresolution approximation of $L^2(\mathbb{R}^2)$. Corresponding to this multiresolution approximation there exists a unique function $\varphi(\boldsymbol{x})\in L^2(\mathbb{R}^2)$, called the scaling function, such that $\{\sqrt{2^l}\,\varphi(\Lambda^l\boldsymbol{x}-\boldsymbol{n}),\ \boldsymbol{n}=[n_1, n_2]^{\mathrm{T}}\in\mathbb{Z}^2\}$ is an orthonormal basis of U_l.

The proof of Result 1 can be found in Appendix A.

Let A_l be the orthogonal projection operator onto U_l. For any 2-D signal $f\in L^2(\mathbb{R}^2)$ the approximation signal at the resolution l is the orthogonal projection A_lf of f onto U_l. By using Result 1 the orthogonal projection A_lf of a function f onto U_l can be obtained as follows:

$$A_lf(\boldsymbol{x})=\sum_{\boldsymbol{n}\in\mathbb{Z}^2}\langle f(\boldsymbol{v}), \sqrt{2^l}\,\varphi(\Lambda^l\boldsymbol{v}-\boldsymbol{n})\rangle \times\sqrt{2^l}\,\varphi(\Lambda^l\boldsymbol{x}-\boldsymbol{n}). \tag{2}$$

The approximation A_lf at the resolution level l of the signal f is characterized by the inner products:

$$A_l^d f[\boldsymbol{n}]=\langle f, S_l[\boldsymbol{n}]\varphi\rangle,\quad \boldsymbol{n}\in\mathbb{Z}^2, \tag{3}$$

where $S_l[\boldsymbol{n}]\varphi(\boldsymbol{x})=2^l\varphi(\Lambda^l\boldsymbol{x}-\boldsymbol{n})$. The 2-D sequence, $A_l^d f[\boldsymbol{n}]$, is called the discrete-time approximation of the function, f, at the resolution level l.

3. Implementation of the multiresolution approximation

Let $\{U_l\}$ be a nonrectangular multiresolution approximation of $L^2(\mathbb{R}^2)$ and $\varphi(\boldsymbol{x})$ be the corresponding scaling function. The set of functions $\{\sqrt{2^{l+1}}\,\varphi(\Lambda^{l+1}\boldsymbol{x}-\boldsymbol{n}),\ \boldsymbol{n}\in\mathbb{Z}^2\}$, is an orthonormal basis of U_{l+1} by Result 1. The function $\varphi(\Lambda^l\boldsymbol{x}-\boldsymbol{n})$ is in $U_l\subset U_{l+1}$. Thus

$$\varphi(\Lambda^l\boldsymbol{x}-\boldsymbol{n}) =2^{l+1}\sum_{\boldsymbol{k}\in\mathbb{Z}^2}\langle\varphi(\Lambda^l\boldsymbol{v}-\boldsymbol{n}), \varphi(\Lambda^{l+1}\boldsymbol{v}-\boldsymbol{k})\rangle \times\varphi(\Lambda^{l+1}\boldsymbol{x}-\boldsymbol{k}). \tag{4}$$

After some algebraic manipulations the inner product in (4) can be rewritten as follows:

$$2^l\langle\varphi(\Lambda^l\boldsymbol{v}-\boldsymbol{n}),\,\varphi(\Lambda^{l+1}\boldsymbol{v}-\boldsymbol{k})\rangle = \langle S_{-1}[\boldsymbol{0}]\varphi,\,S_0[\boldsymbol{k}-\Lambda\boldsymbol{n}]\varphi\rangle. \tag{5}$$

We note that the right-hand side of (5) is independent of the resolution level l. By computing the inner product of $f(x)$ with both sides of (4) and after some algebraic manipulations we obtain the relation between the sequence $A_l^d f$ and the sequence $A_{l+1}^d f$ as follows:

$$A_l^d f[\boldsymbol{n}] = \sum_{\boldsymbol{k}\in\mathbb{Z}^2} h[\boldsymbol{k}-\Lambda\boldsymbol{n}]A_{l+1}^d f[\boldsymbol{k}], \tag{6}$$

where the 2-D sequence $h[n_1, n_2]=h[\boldsymbol{n}]=\langle S_{-1}[\boldsymbol{0}]\varphi, S_0[\boldsymbol{n}]\varphi\rangle$, which can be considered as a 2-D linear time-invariant filter. Equation (6) implies that the discrete-time approximation signal $A_l^d f$ can be obtained by convolving $A_{l+1}^d f$ with the filter $h_0[\boldsymbol{n}]=h[-n_1, -n_2]$ and quincunx down-sampling. The quincunx down-sampling is carried out after the filtering operation. Equation (6) is graphically described in Fig. 1. The matrix Λ is called the quincunx downsampling matrix [2].

As a consequence of (4) one can also show that

$$\hat{\varphi}(\Lambda\omega)=H(\omega)\hat{\varphi}(\omega), \tag{7}$$

where $\hat{\varphi}$ is the continuous-time Fourier transform (FT) of φ, $H(\omega)$ is the 2-D discrete-time FT (the frequency response) of the sequence (the filter) $h[\boldsymbol{n}]$, and $\omega=(\omega_1, \omega_2)$ with an abuse of notation.

The set of functions $\{\varphi(\boldsymbol{x}-\boldsymbol{n}),\ \boldsymbol{n}\in\mathbb{Z}^2\}$ is orthonormal, if and only

$$\sum_{\boldsymbol{k}\in\mathbb{Z}^2}|\hat{\varphi}(\omega+2\boldsymbol{k}\pi)|^2=1 \quad \forall\omega_1, \omega_2 \tag{8}$$

or

$$\sum_{\boldsymbol{k}\in\mathbb{Z}^2}|\hat{\varphi}(\Lambda\omega+2\boldsymbol{k}\pi)|^2=1 \quad \forall\omega_1, \omega_2. \tag{9}$$

By using (7) and (9), and after some algebraic manipulations, we obtain the following condition for the filter $h[\boldsymbol{n}]$:

$$|H(\omega)|^2+|H(\omega+\pi[1\quad 1]^{\mathrm{T}})|^2=1. \tag{10}$$

Also $|\int\varphi(\boldsymbol{x})\,d\boldsymbol{x}|=|\hat{\varphi}(0,0)|=1$ implies that $|H(0,0)|=1$. In the next result, we describe the conditions that the filter $H(\omega)$ satisfies.

RESULT 2. Let $\varphi(\boldsymbol{x})$ be a scaling function and let $h[\boldsymbol{n}]$ be the 2-D discrete-time filter with impulse response $h[\boldsymbol{n}]=\langle S_{-1}[\boldsymbol{0}]\varphi, S_0[\boldsymbol{n}]\varphi\rangle$. The frequency response $H(\omega)$ of $h[\boldsymbol{n}]$ satisfies the following conditions:

(i) $|H(\omega)|^2+|H(\omega+\pi[1\ \ 1]^{\mathrm{T}})|^2=1$,

(ii) $|H(0,0)|=1$, and

(iii) $h[\boldsymbol{n}]$ decays exponentially as $n_1, n_2\to\infty$.

Conversely, if $H(\omega)$ satisfies the conditions (i)–(iii), and

(iv) $H(\omega)\neq 0$ for $\omega\in\{|\omega_1|+|\omega_2|<\pi\}$, then the continuous-time Fourier transform (FT) defined by

$$\hat{\varphi}(\omega)=\prod_{p=1}^{\infty}H(\Lambda^{-p}\omega) \tag{11}$$

is the FT of the scaling function $\varphi(\boldsymbol{x})$.

The convergence of (11) is not always assured [7]. If the function $\varphi(\boldsymbol{x})$ obtained by using (11) is regular, i.e., converges to a 'smooth' function [7] then the sequence of vector spaces $\{U_l\}_{l=-\infty}^{\infty}$ constructed from $\varphi(\boldsymbol{x})$ is a multiresolution approximation of $L^2(\mathbb{R}^2)$.

We have already proved properties (i) and (ii) of Result 2. The formal proof of this result can be established as in [13].

The 2-D discrete-time filters satisfying conditions (i)–(iv) can be found in [2]. These filters are IIR filters with diamond-shaped passbands.

4. The wavelet representation

The difference of information between the resolution levels l and $l+1$ is characterized by a signal called the detail signal at the resolution level l. In this section, we describe the construction of the detail signal and define the nonrectangular wavelet representation of a signal.

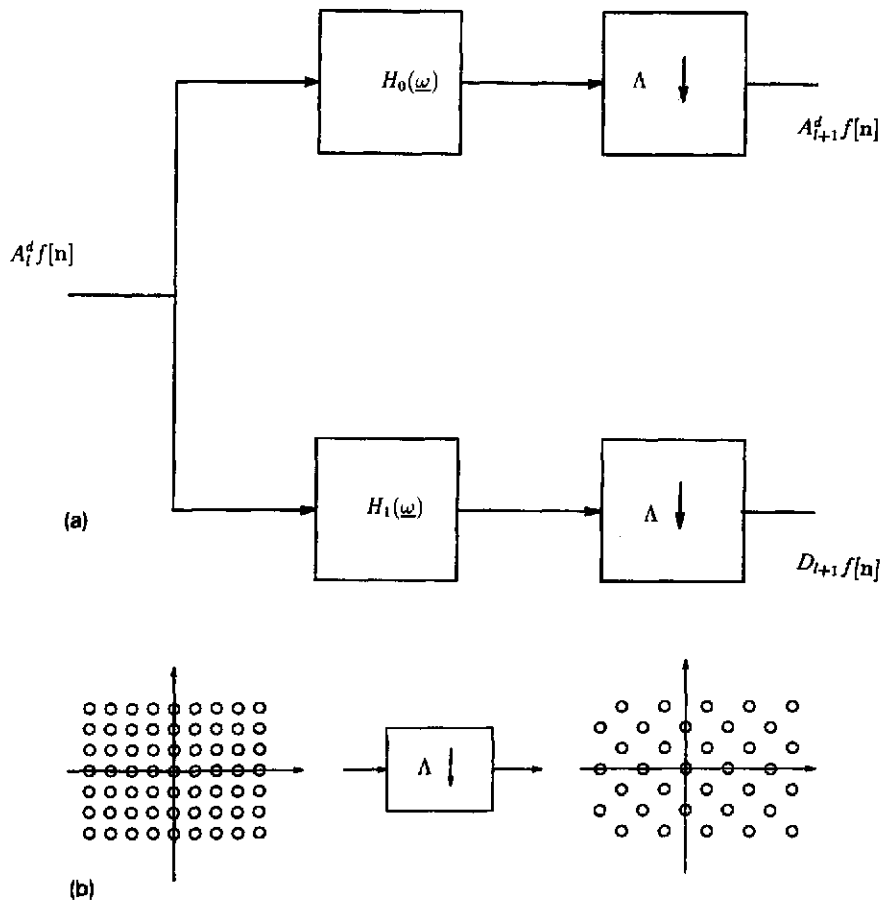

Fig. 1. (a) Subband decomposition structure to obtain $A^d_{l+1}f[n]$ and $D_{l+1}f[n]$ from $A^d_l f[n]$. (b) Action of the quincunx downsampling block to a rectangularly sampled input $v[n]$ (the output signal $u[n]=v[\Lambda n]$ is a quincunx sampled signal).

Let us define a sequence of subspaces, $\{O_l\}_{l=-\infty}^{\infty}$, where O_l satisfies the following two conditions:

(i) O_l is orthogonal to U_l, and

(ii) $O_l \oplus U_l = U_{l+1}$.

An orthonormal basis can be constructed for O_l by scaling and translating a function, $\psi(x)$, which is called the wavelet.

RESULT 3. The set of functions $\{\sqrt{2^l}\,\psi(\Lambda^l x-n), n\in\mathbb{Z}^2\}$ is an orthonormal basis of O_l, if

$$\hat{\psi}(\underline{\omega})=G(\Lambda^{-1}\underline{\omega})\hat{\varphi}(\Lambda^{-1}\underline{\omega}), \tag{12}$$

where $G(\underline{\omega})=H(\underline{\omega}+\pi[1\ \ 1]^T)$ and $\hat{\psi}(\underline{\omega})$ is the FT of $\psi(x)$. Furthermore, $\{\psi_l(x-n), l\in\mathbb{Z}, n\in\mathbb{Z}^2\}$ is an orthonormal basis of $L^2(\mathbb{R}^2)$. The function $\psi(x)$ is called the orthonormal nonrectangular wavelet.

In this section, we give the key steps of the proof of Result 3. The formal proof can be established as in [13].

We can express $\psi(\Lambda^{-1}x)$ in terms of $\{\varphi(x-n), n\in\mathbb{Z}^2\}$ because $\psi(\Lambda^{-1}x)\in O_{-1}\subset U_0$, i.e.,

$$\psi(\Lambda^{-1}x)=\sum_{k\in\mathbb{Z}^2}\langle\psi(\Lambda^{-1}v),\varphi(v-k)\rangle\varphi(x-k). \tag{13}$$

By computing the Fourier transform of both sides of (13) we obtain

$$\hat{\psi}(\Lambda\underline{\omega})=G(\underline{\omega})\hat{\varphi}(\underline{\omega}), \tag{14}$$

where

$$G(\omega)=\sum_{n\in\mathbb{Z}^2}\langle S_{-1}[\mathbf{0}]\psi, S_0[n]\varphi\rangle\, e^{-j\omega^T n}, \qquad (15)$$

which can be considered as the frequency response of the 2-D discrete-time filter, $g[n]=\langle S_{-1}[\mathbf{0}]\psi, S_0[n]\varphi\rangle$.

Orthogonality of the set of functions $\{\psi(x-n), n\in\mathbb{Z}^2\}$ implies that

$$\sum_{k\in\mathbb{Z}^2}|\hat{\psi}(\omega+2k\pi)|^2=1 \quad \forall\omega_1,\omega_2. \qquad (16)$$

B using (8), (14) and (16) it can be shown that

$$|G(\omega)|^2+|G(\omega+[1\quad 1]^T\pi)|^2=1. \qquad (17)$$

Also, O_{-1} is orthogonal to U_{-1} by definition, thus $\sqrt{2^{-1}}\,\psi(\Lambda^{-1}x-n)$ is orthogonal to $\sqrt{2^{-1}}\,\varphi(\Lambda^{-1}x-k)$ for all $k, n\in\mathbb{Z}^2$. This condition is equivalent to

$$\sum_{k\in\mathbb{Z}^2}\hat{\varphi}(\omega+2k\pi)\hat{\psi}^*(\omega+2k\pi)=0. \qquad (18)$$

By inserting (14) into (18) and using (8) we obtain a condition which must be satisfied by the filters $H(\omega)$ and $G(\omega)$, i.e.,

$$H(\omega)G(\omega)+H(\omega+[1\quad 1]^T\pi)\times G(\omega+[1\quad 1]^T\pi)=0. \qquad (19)$$

One can prove that the necessary conditions (17) and (19) are sufficient to prove that the set of functions, $\{\sqrt{2^l}\,\psi(\Lambda^l x-n), n\in\mathbb{Z}^2\}$, is an orthonormal basis of O_l. Conditions (10), (17) and (19) are perfect reconstruction conditions of a nonrectangular subband decomposition filter bank [2]. In [2] the filter $G(\omega)$ is chosen as follows:

$$G(\omega)=H(\omega+[1\quad 1]^T\pi). \qquad (20)$$

The IIR filters designed in [2] satisfy the conditions (10), (17) and (19). In the next section, we describe the filters $H(\omega)$ and $G(\omega)$ in detail.

By using Results 2 and 3 one can construct a nonrectangular wavelet orthonormal basis of $L^2(\mathbb{R}^2)$ from a nonrectangular filter bank, if the right-hand side of (11) converges.

Let us now describe the discrete-time detail signals for a given function $f\in L^2(\mathbb{R}^2)$. Let P_l^o be the projection operator onto O_l. The projection $P_l^o f$ of the function f onto O_l is given as follows:

$$P_l^o f(x)=\sum_{n\in\mathbb{Z}^2}\langle f(v), \sqrt{2^l}\,\psi(\Lambda^l v-n)\rangle \times\sqrt{2^l}\,\psi(\Lambda^l x-n). \qquad (21)$$

We call the projection $P_l^o f(x)$ the detail signal of $f(x)$ at the resolution l. The detail signal is characterized by the 2-D sequence

$$D_l f[n]=\langle f, S_l[n]\psi\rangle, \quad n\in\mathbb{Z}^2, \qquad (22)$$

where $S_l[n]\psi(x)=2^l\psi(\Lambda^l x-n)$. The 2-D sequence defined in (22) is called the discrete-time detail signal at the resolution level l.

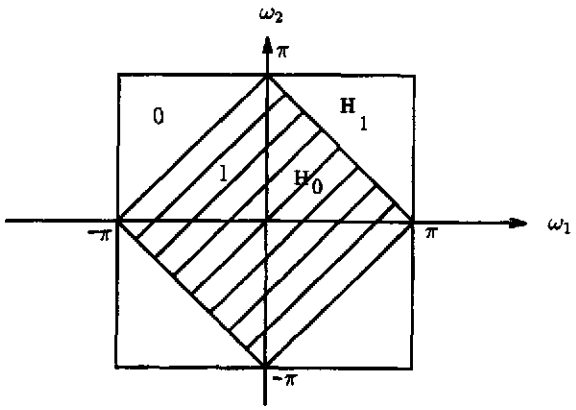

Fig. 2. Ideal diamond-shaped frequency response of the filter H_0 (H_1 is a highpass filter with a diamond-shaped stopband).

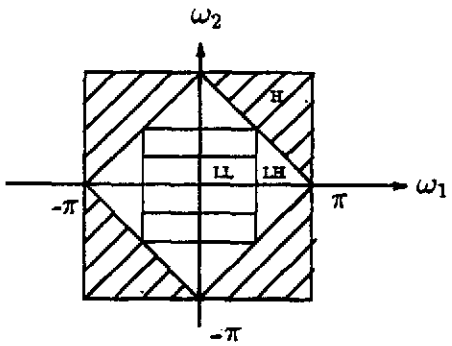

Fig. 3. Decomposition of the frequency domain by the wavelet representation $\{A_{-2}^d f; D_{-2}f, D_{-1}f\}$.

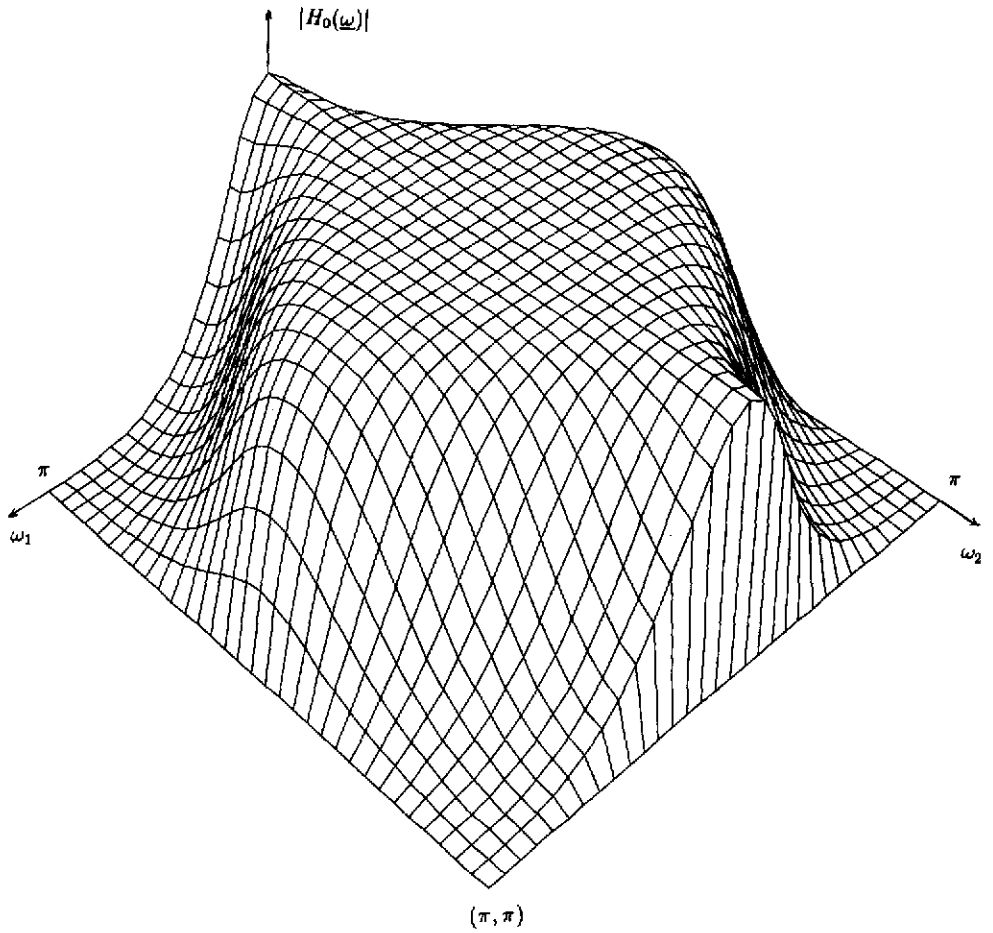

Fig. 4. Magnitude response of the lowpass filter $H_0(\underline{\omega})$.

The function $\psi_l \in U_{l+1}$ since $O_l \subset U_{l+1}$. By using this fact we can show that

$$D_l f[\underline{n}] = \sum_{\underline{k} \in \mathbb{Z}^2} g[\underline{k} - \Lambda \underline{n}] A^d_{l+1} f[\underline{n}], \tag{23}$$

where the sequence $g[\underline{n}]$ is the impulse response of the filter $G(\underline{\omega})$ defined in (15). Thus the discrete detail signal $D_l f$ can be obtained by convolving $A^d_{l+1} f$ with the discrete filter $h_1[\underline{n}] = g[-n_1, -n_2]$ and quincunx down-sampling. These operations are graphically described in Fig. 1. By using (6) and (23) we can show that the discrete-time detail signal $D_l f$ and the approximation signal $A_l f$ can be obtained from $A^d_{l+1} f$ by using the filter bank structure described in [1, 2] (see Fig. 1) The filter pair $H_0(\underline{\omega})$ and $H_1(\underline{\omega})$ decompose the frequency domain in a nonrectangular fashion. Since $H_1(\underline{\omega}) = H_0(\omega_1 + \pi, \omega_2 + \pi)$ the stopband of $H_1(\underline{\omega})$ is a diamond-shaped region (passband of $H_0(\underline{\omega})$) in the frequency domain.

The discrete-time signal $A^d_l f$ can be represented by the detail signals at resolutions $k = K$, $K+1, \ldots, l-1$ and $A^d_K f$, $K < l$. We call the set of signals

$$\{A^d_K f; D_k f, k = K, K+1, K+2, \ldots, l-1\} \tag{24}$$

the nonrectangular wavelet representation of $A^d_l f$. The set of signals in (24) uniquely determines $A^d_l f$. This wavelet representation of $A^d_l f$ can be recursively obtained from $A^d_l f$ by using the filter

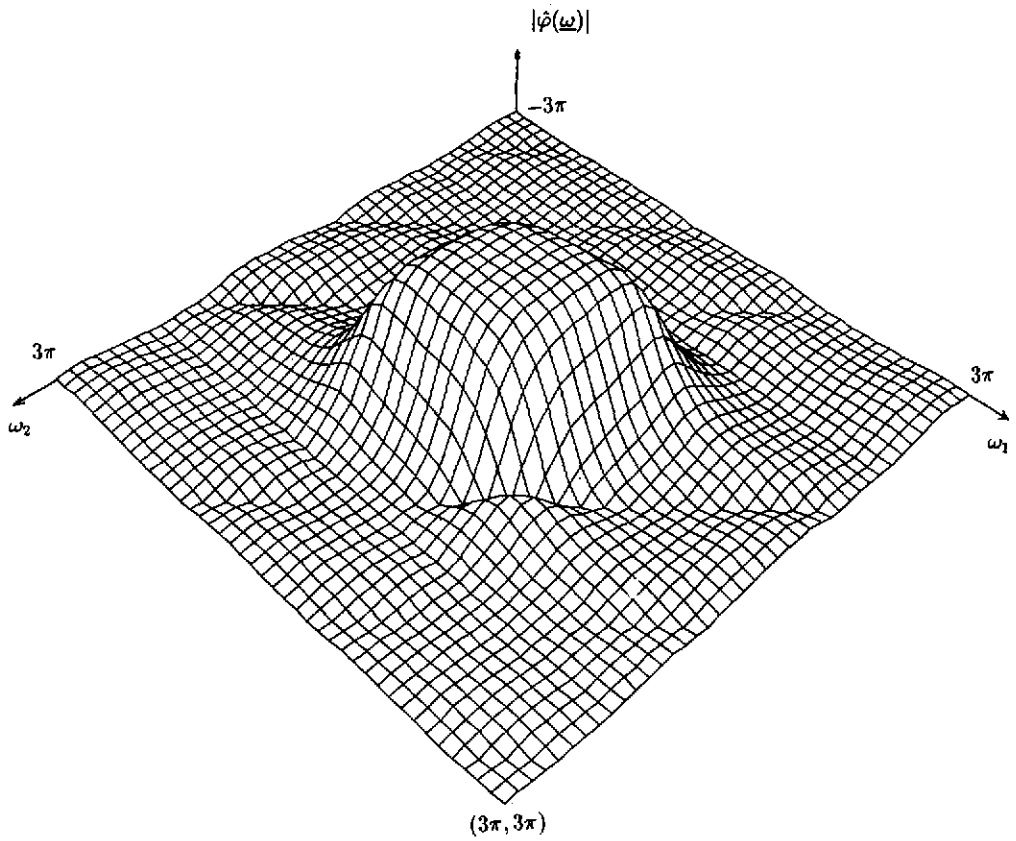

Fig. 5. Magnitude response of the smoothing function after the eighth iteration of (11).

bank structure shown in Fig. 1 or equivalently via (6) and (23).

The reconstruction of $A_l^d f$ from one of its nonrectangular wavelet representation can be carried out by using the reconstruction filter bank of [2] in a tree-structured manner. The signals $A_K^d f$ and $D_K f$ are first upsampled according to the matrix Λ, i.e.,

$$y_a^K[\boldsymbol{n}] = \begin{cases} A_K^d f[\boldsymbol{n}] & \text{if } \Lambda \boldsymbol{n} \in \mathbb{Z}^2, \\ 0 & \text{otherwise,} \end{cases} \tag{25}$$

and

$$y_d^K[\boldsymbol{n}] = \begin{cases} D_K f[\boldsymbol{n}] & \text{if } \Lambda \boldsymbol{n} \in \mathbb{Z}^2, \\ 0 & \text{otherwise,} \end{cases} \tag{26}$$

where the signals $y_a^K[\boldsymbol{n}]$ and $y_d^K[\boldsymbol{n}]$ are the upsampled signals. This operation corresponds to an upsampling (quincunx upsampling) by a factor of two. The signals, $y_a^K[\boldsymbol{n}]$ and $y_d^K[\boldsymbol{n}]$, are filtered by $2H_0(-\underline{\omega})$ and $2H_1(-\underline{\omega})$, respectively and the outputs of the filters are summed. In this way, we obtain $A_{K+1}^d f$. We continue doing this process recursively until $A_l^d f$ is obtained.

5. Image coding

In this section, we present the image coding method based on nonrectangular wavelet representation described in Section 4.

Let $u[\boldsymbol{n}]$ be a digital image to be compressed. We assume that this image is the discrete approximation at the resolution level 0 of the 2-D continuous-time signal, $f(\boldsymbol{x})$, i.e., $u[\boldsymbol{n}] = A_0^d f(\boldsymbol{x})$. In this image

Table 1
SNR and bit-rates for Lena image

DCT block size and scaling factor for low image		Filter 1		Filter 2	
		Bit-rate (bits/pel)	SNR (dB)	Bit-rate (bits/pel)	SNR (dB)
8 × 8	1	0.89	36.7	0.89	37.0
8 × 8	2	0.66	36.0	0.62	36.2
16 × 16	1	0.66	36.0	0.62	36.1

Table 2
SNR and bit-rates for Kiel harbour image

DCT block size and scaling factor for low image		Filter 1		Filter 2	
		Bit-rate (bits/pel)	SNR (dB)	Bit-rate (bits/pel)	SNR (dB)
8 × 8	1	1.57	31.8	1.57	30.7
8 × 8	1[a]	—	—	—	—
8 × 8	2	1.36	31.5	1.36	30.2
16 × 16	1	1.37	31.5	1.37	30.4

[a] With finer quantization of outer bands than the previous row.

Table 3
SNR and bit-rates for Barbara image

DCT block size and scaling factor for low image		Filter 1		Filter 2	
		Bit-rate (bits/pel)	SNR (dB)	Bit-rate (bits/pel)	SNR (dB)
8 × 8	1	1.34	33.9	1.28	34.9
8 × 8	2	1.1	34.0	1.04	34.2
16 × 16	1	1.1	33.9	1.01	34.2

coding technique, the following wavelet representation of $u[n]$ is constructed:

$$\{A^d_{-2}f;\, D_{-2}f,\, D_{-1}f\}. \tag{27}$$

Although the signal $u[n]$ is rectangularly sampled the subsignals $D_{-1}f$ and $A^d_{-1}f$ are quincunx sampled, and $D_{-2}f$ and $A^d_{-2}f$ are again rectangularly sampled. This is because of the fact that if quincunx downsampling is applied twice to a rectangularly sampled signal then the result is a rectangularly sampled signal, and a sampling rate reduction by a factor of four is achieved in this way. We also note that $\Lambda^2 = 2I$, where $2I$ is the rectangular downsampling matrix [1]. The ideal frequency decomposition of the frequency domain by (14) is shown in Fig. 3.

In order to generate these subsignals we use the nonrectangular subband decomposition filter bank structure of [2] shown in Fig. 1, where we use the IIR filters

$$H_i(\omega) = \tfrac{1}{2}[1 + (-1)^i e^{j\omega_1} T(\omega_1 + \omega_2) T(\omega_1 - \omega_2)],$$
$$i = 0, 1, \tag{28}$$

where

$$T(\omega) = \frac{a_1 e^{j\omega} + 1}{a_1 + e^{j\omega}} \tag{29}$$

is an all-pass section. In this filter bank exact reconstruction in the absence of coding errors is provided [2]. We note that conditions (i)–(iii) of Results 2 and 3 are satisfied. The ideal frequency response of the lowpass filter H_0 is shown in Fig. 2 and decomposition of the frequency domain by (14) is shown in Fig. 3. In the simulation examples, the filters corresponding to the coefficients $a_1 = 1/3$ (Filter 1) and $a_1 = 1/4$ (Filter 2) are used. The magnitude response of the Filter 2 is shown in Fig. 4 and the magnitude response of $\prod_{p=1}^{8} H_0(\Lambda^{-p}\omega)$ is

Fig. 6. Lena image at 0.89 bits/pel with SNR = 37.1 dB.

shown in Fig. 5. Although we cannot establish the formal convergence proof of (11) it can be observed from Fig. 5 that $\prod_{p=1}^{\infty} H_0(\Lambda^{-p}\omega)$ converges to a smooth function. Similar plots can also be obtained for Filter 1. A convergence proof for the FIR filter case could not be formally established in [10], either.

The filters, $H_i(\omega)$, $i=0, 1$, are suited for fast implementation as the filter coefficients are integers. The IIR filters have approximately linear phase characteristics in their passbands so that the lower-resolution lowband subsignal $A^d_{-2}f$ does not exhibit phase distortion associated with IIR filters.

In many images, the lowband subsignal $A^d_{-2}f$ contains most of the signal energy and significant information, and also represents a lower-resolution version of the original image. In view of this, the lowband subsignal has to be faithfully coded. The high correlation among neighboring samples of $A^d_{-2}f$ makes it a good candidate for efficient predictive and transform coding. Here we have chosen to employ a variant of Discrete Cosine Transform coding method of [6]. The algorithm described in [6] with some modifications was applied to blocks of data of size 8×8 or 16×16. The transform coefficients are scanned in a zig-zag manner, and are quantized by rounding of suitably scaled coefficients. A large portion of the quantized coefficients are observed to be zero. The values of the nonzero coefficients are coded with an amplitude lookup table, and their locations are coded using a runlength table.

The high frequency subsignals $D_{-1}f$ and $D_{-2}f$ are coded using first a deadzone quantizer for data compression. These subsignals are then coded noiselessly by employing runlength coding for runs of zero values using a lookup table and the nonzero values are amplitude coded using a Huffman code based lookup table. The quantizer can be chosen according to the statistics of the subsignals and their visual impact. It was found that a coarser quantizer can be used in the outermost band subsignal $D_{-1}f$ and a finer quantizer can be used on the inner high frequency band subsignal $D_{-2}f$. The deadzones can also be chosen in a similar manner, i.e., deadzone of the quantizer which codes $D_{-1}f$ is larger than the quantizer of $D_{-2}f$. However, for more demanding images such as HDTV signals,

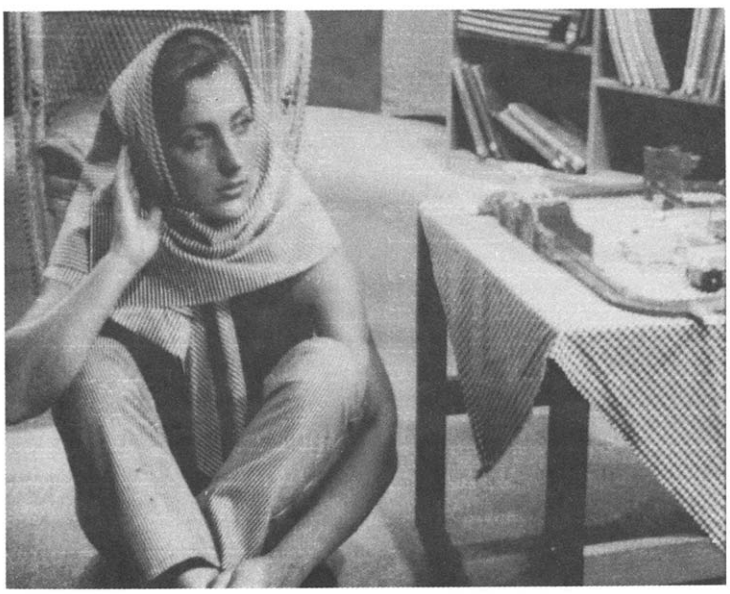

Fig. 7. Barbara image at 1.24 bits/pel with SNR = 35.3 dB.

one may have to use smaller deadzones. The quantizers used beyond the deadzone were almost uniform with slightly smaller quantization intervals used for low magnitude samples. After the deadzone quantization, most of the test images have a significantly reduced number of nonzero values. The information on the location of these nonzero values can be efficiently coded using runlength coding [4].

The above image coding procedure was applied to several test images and the results obtained here are focused on Lena, Barbara and Kiel Harbour images. The sizes of these images are 512×512, 672×576 and 720×576, respectively.

The coding results are presented in Tables 1–3. Among the parameters changed were the filter coefficients ($a_1 = 1/3$ and $1/4$), the quantization of outer bands, the DCT block size, and the rounding procedure. These results are comparable to those obtained in the case of rectangular subband coding [3]. The decoded images using Filter 1 are shown in Figs. 6–8.

The main advantage of nonrectangular processing is the hierarchy created by the partition into two subbands without any horizontal or vertical bias and filter characteristics matching those of human visual perception. This feature is attractive in situations where there is a loss of the high band information due to reasons such as network congestion. To see the effect of the loss of the high band information, we applied the Barbara and Kiel Harbour signals to the analysis filter bank and discarded the outermost band. The remaining information was used to reconstruct the signal. The decoded Barbara image without outer band information is shown in Fig. 9. The SNR for this image is 30.3 dB. In Fig. 10 the decoded Barbara image with the loss of high horizontal rectangular subband is shown. In this case the SNR is 27.2 dB. Aliasing effects are more disturbing in Fig. 10.

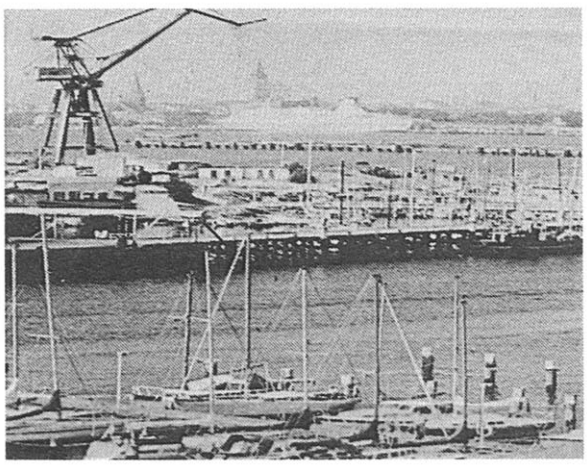

Fig. 8. Kiel Harbour image at 2.04 bits/pel with SNR = 37.5 dB.

6. Conclusions

In this paper we described a nonrectangular multiresolution wavelet representation for 2-D signals and an image coding method which can compress both quincunx and rectangularly sampled images. This wavelet representation achieves a diamond-shaped decomposition of the frequency domain. The quincunx wavelet representation can be implemented by a class of IIR filter banks whose regularity is experimentally observed. Although we could not prove the convergence in this paper, we believe that the regularity proof of the IIR filter bank can be formally established.

The issues of generalization of this framework to other 2-D sampling geometries will also be explored.

Appendix A. Proof of Result 1

In this appendix, we show the main steps of the proof of Result 1 for $l = 0$.

Property (5) of the nonrectangular multiresolution approximation definition states that there exists an isomorphism, I, from U_0 onto $\ell^2(\mathbb{Z}^2)$. Thus there is a function, $w(\boldsymbol{x}) \in U_0$ such that $\mathrm{I}(w(\boldsymbol{x})) = \delta[\boldsymbol{n}]$ which is the 2-D discrete-time Dirac-delta sequence. Also, $\mathrm{I}(w(\boldsymbol{x}-\boldsymbol{k})) = \delta[\boldsymbol{n}-\boldsymbol{k}]$ for all $\boldsymbol{k} \in \mathbb{Z}^2$. Since $\{\delta[\boldsymbol{n}-\boldsymbol{k}], \boldsymbol{k} \in \mathbb{Z}^2\}$ is a basis of $\ell^2(\mathbb{Z}^2)$ the set of functions, $\{w(\boldsymbol{x}-\boldsymbol{k}), \boldsymbol{k} \in \mathbb{Z}^2\}$, is a basis of

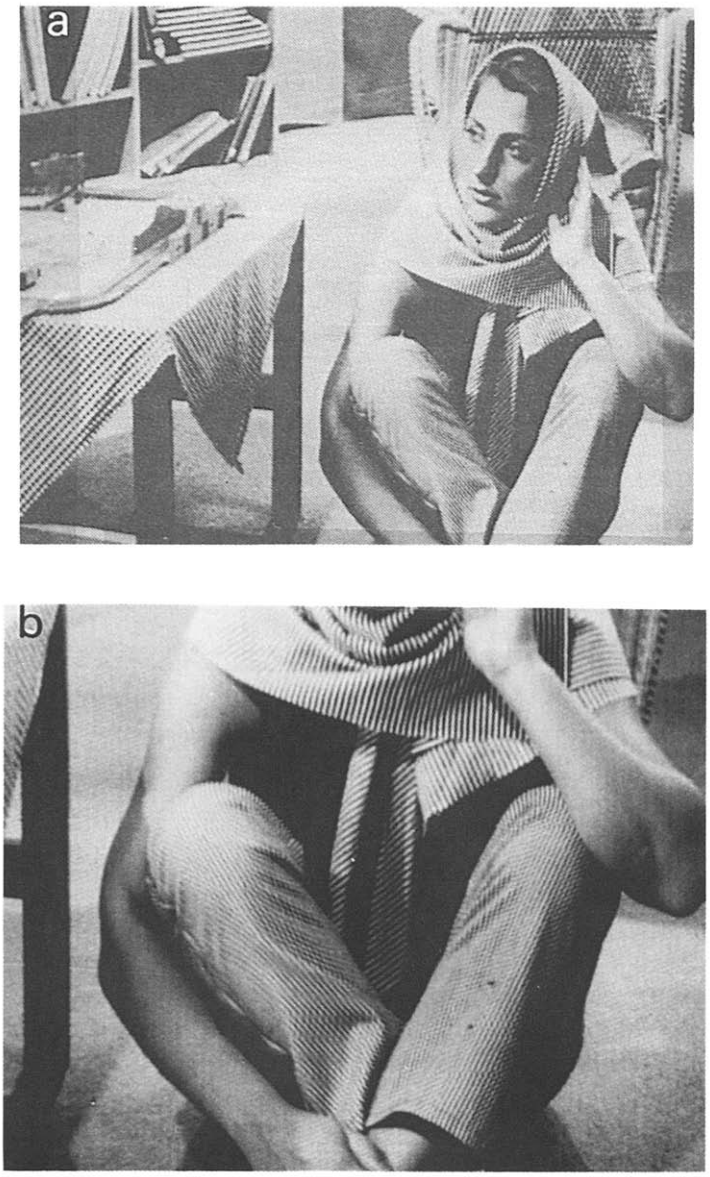

Fig. 9 (a) Decoded Barbara image without outer band, $D_{-1}f$: SNR = 30.3 dB. (b) Details of pants and the scarf in Fig. 9(a).

U_0. Thus any $f(x) \in U_0$ can be expressed as follows:

$$f(x) = \sum_{k \in \mathbb{Z}^2} b_k w(x-k). \quad \text{(A.1)}$$

By computing the Fourier transform of both sides of (A.1) we get

$$\hat{f}(\omega) = B_f(\omega)\hat{w}(\omega), \quad \text{(A.2)}$$

where $B_f(\omega) = \sum_{k \in \mathbb{Z}^2} b_k e^{-j\omega^T k}$. The L^2 norm of $f(x)$ is given by

$$\|f\|^2 = \int |\hat{f}(\omega)|^2 \, d\omega$$

$$= \int_0^{2\pi} \int_0^{2\pi} |B_f(\omega)|^2 \times \sum_{k \in \mathbb{Z}^2} |\hat{w}(\omega + 2k\pi)|^2 \, d\omega. \quad \text{(A.3)}$$

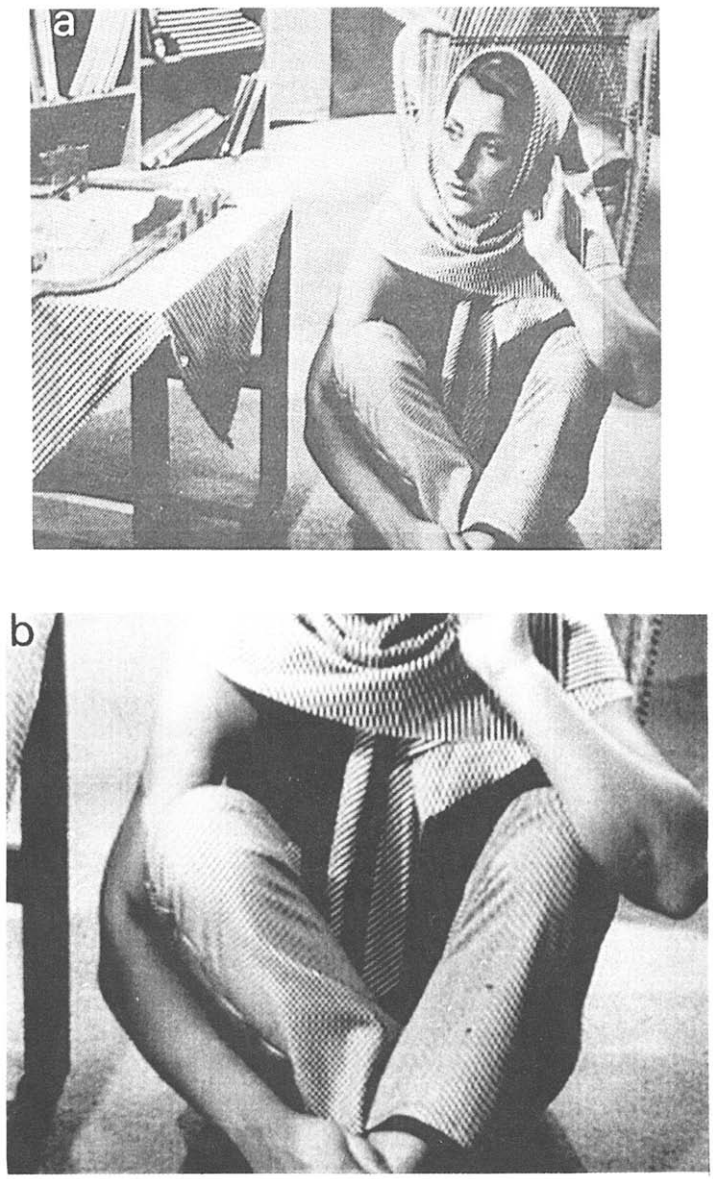

Fig. 10. (a) Decoded Barbara image without high-horizontal band of the rectangular decomposition: SNR = 27.2 dB. (b) Details of pants and the scarf in Fig. 10(a). Aliasing effects are clearly observable.

Since I is an isomorphism the L^2 norm and the ℓ^2 norm are equivalent to each other on U_0. Thus there exist two real constants, c_1 and c_2, such that

$$c_1 \leqslant \sqrt{\left| \sum_{k \in \mathbb{Z}^2} \hat{w}(\omega + 2k\pi) \right|^2} \leqslant c_2. \qquad \text{(A.4)}$$

In order to compute the scaling function $\varphi(x) \in U_0$, we orthonormalize the basis $\{w(x-k),\ k \in \mathbb{Z}^2\}$ by using the Poisson formula. The assumption of the orthonormality of the set of functions $\{\varphi(x-k),\ k \in \mathbb{Z}^2\}$ implies that

$$\sum_{k \in \mathbb{Z}^2} |\hat{\varphi}(\omega + 2k\pi)|^2 = 1 \quad \forall \omega_1, \omega_2. \qquad \text{(A.5)}$$

Also from (A.2) there is a 2π-periodic function $B_\varphi(\omega)$ corresponding to $\varphi(x)$ such that

$$\hat{\varphi}(\omega) = B_\varphi(\omega)\hat{w}(\omega), \tag{A.6}$$

and by inserting (A.6) into (A.5) we get

$$B_\varphi(\omega) = \left(\sum_{k \in \mathbb{Z}^2} |\hat{w}(\omega + 2k\pi)|^2 \right)^{-1/2}, \tag{A.7}$$

which is a bounded function of ω and $B_\varphi(\omega) \in L^2([0, 2\pi])$. Therefore, (A.6) and (A.7) define a function $\varphi(x)$ such that $\{\varphi(x-k), k \in \mathbb{Z}^2\}$ is an orthonormal basis of U_0.

Acknowledgments

The author thanks Dr. Rashid Ansari, Bellcore, and Prof. Cemal Yalabik, Department of Physics, Bilkent University, for their help and comments.

References

[1] R. Ansari and S. Lee, Two-dimensional nonrectangular interpolation, decimation and filter banks, Technical Report, Bell Communications Research, USA, 1988.

[2] R. Ansari and C.L. Lau, "Two-dimensional IIR filters for exact reconstruction in tree-structured sub-band decomposition", *Electron. Lett.*, Vol. 23, June 1987, pp. 633–634.

[3] R. Ansari and D. Le Gall, "Subband coding of HDTV signals" in: J. Woods, ed., *Subband Image Coding*, Kluwer Academic Publishers, Hingham, MA, 1991.

[4] R. Ansari, A.E. Çetin and S. Lee, "Subband coding of images using nonrectangular filter banks", *Proc. SPIE Conf. on Applications of Image Processing XI*, San Diego, August 1988.

[5] P. Burt and E. Adelson, "The Laplacian pyramid as a compact image code", *IEEE Trans. Comm.*, Vol. 31, 1983, pp. 532–540.

[6] W.-H. Chen and W.K. Pratt, "Scene adaptive coder", *IEEE Trans. Comm.*, Vol. 32, March 1984, pp. 225–232.

[7] I. Daubechies, "Orthonormal bases of compactly supported wavelets", *Comm. Pure Appl. Math.*, Vol. 41, November 1988, pp. 909–996.

[8] E. Dubois, "The sampling and reconstruction of time-varing imagery with applications in video systems", *Proc. IEEE*, Vol. 73, 1985, pp. 502 522.

[9] J.C. Feaveau, "Analyse multirésolution pour les images avec un facteur de résolution $\sqrt{2}$", *Traitement du Signal*, Vol. 7, 1990, pp. 117–128.

[10] J. Kovacevic and M. Vetterli, "Nonseparable multidimensional perfect reconstruction filter banks and wavelet for R^n", *IEEE Trans. Inform. Theory*, Vol. 38, March 1922, pp. 533 555.

[11] J. Kovacevic, M. Vetterli and G. Karlsson, "Design of multidimensional filter banks for nonseparable sampling", *Proc. Internat. Symp. Circuits and Systems '90*, IEEE Press, New Orleans, 1990.

[12] S. Mallat, "A theory of multiresolution signal decomposition: Wavelet representation", *IEEE Trans. Pattern Anal. Machine Intell.*, Vol. 11, July 1989, pp. 674–693.

[13] S. Mallat, "Multiresolution approximation and wavelet orthonormal bases of L^2", *Trans. Amer. Math. Soc.*, Vol. 315, 1989, pp. 69 87.

[14] Y. Meyer, *Ondellettes et Opérateurs*, Hermann, Paris, 1990.

[15] E. Viscito and J. Allebach, "The analysis and design of multidimensional FIR perfect reconstruction filter banks for arbitrary sampling lattices", *IEEE Trans. Circuits and Systems*, Vol. 38, January 1991, pp. 29 42.

[16] J.W. Woods, ed., *Subband Image Coding*, Kluwer, Norwell, MA, 1991.